Geomorphic significance of postglacial bedrock scarps on normal-fault footwalls

Gregory E. Tucker,[1] Scott W. McCoy,[1] Alexander C. Whittaker,[2] Gerald P. Roberts,[3] Stephen T. Lancaster,[4] and Richard Phillips[5]

Received 25 August 2010; revised 4 January 2011; accepted 10 January 2011; published 19 March 2011.

[1] The existence of well-preserved Holocene bedrock fault scarps along active normal faults in the Mediterranean region and elsewhere suggests a dramatic reduction in rates of rock weathering and erosion that correlates with the transition from glacial to interglacial climate. We test and quantify this interpretation using a case study in the Italian Central Apennines. Holocene rates are derived from measurements of weathering-pit depth along the Magnola scarp, where previous cosmogenic ^{36}Cl analyses constrain exposure history. To estimate the average hillslope erosion rate over ~10^5 years, we introduce a simple geometric model of normal-fault footwall slope evolution. The model predicts that the gradient of a weathering-limited footwall hillslope is set by fault dip angle and the ratio of slip rate to erosion rate; if either slip or erosion rate is known, the other can be derived. Applying this model to the Magnola fault yields an estimated average weathering rate on the order of 0.2–0.4 mm/yr, more than 10 times higher than either the Holocene scarp weathering rate or modern regional limestone weathering rates. A numerical model of footwall growth and erosion, in which erosion rate tracks the oxygen-isotope curve, reproduces the main features of hillslope and scarp morphology and suggests that the hillslope erosion rate has varied by about a factor of 30 over the past one to two glacial cycles. We conclude that preservation of carbonate fault scarps reflects strong climatic control on rock breakdown by frost cracking.

Citation: Tucker, G. E., S. W. McCoy, A. C. Whittaker, G. P. Roberts, S. T. Lancaster, and R. Phillips (2011), Geomorphic significance of postglacial bedrock scarps on normal-fault footwalls, *J. Geophys. Res.*, *116*, F01022, doi:10.1029/2010JF001861.

1. Introduction

[2] Climate influences the rate and style of hillslope evolution, and consequently the supply of sediment to rivers, glaciers, and ultimately sedimentary basins [e.g., *Bull*, 2001; *Leeder et al.*, 1998]. Yet the strength and nature of the connection between climate and hillslope erosion remain poorly understood at a quantitative level. Process-response models predict a strong link between weathering, erosion, and climate properties such as precipitation [e.g., *Kirkby and Cox*, 1995; *Tucker and Slingerland*, 1997; *Coulthard and Kirkby*, 2002] and temperature [e.g., *Anderson*, 1998; *Hales and Roering*, 2005]. Such links manifest themselves, for example, in changing rates and patterns of landform development between glacial and interglacial cycles [e.g., *Hancock and Anderson*, 2002]. Some have argued that the climatic control on rates of sediment production and delivery is strong enough to account for an apparent worldwide increase in sediment delivery to basins beginning in the late Cenozoic [*Zhang et al.*, 2001; *Molnar*, 2004]. Yet other studies show remarkably little correlation between denudation and climate. For example, in the Sierra Nevada, USA, *Riebe et al.* [2001] found surprisingly little variation in chemical denudation rate across a wide range in mean temperature and precipitation. Likewise, several studies of modern sediment yield suggest that particulate flux is more strongly correlated with topographic relief than with climatic attributes such as annual precipitation [*Milliman and Syvitski*, 1992; *Hovius*, 1998; *Summerfield and Hulton*, 1994]. Thus, one is faced with something of a conundrum: evidence from some models and some landscapes suggests a powerful climatic control on hillslope evolution and sediment production, while other studies appear to show little correlation. This points to a need for targeted studies that isolate geomorphic sensitivity to climate in particular environments, landform types, and processes.

[3] Here we take advantage of a type of natural experiment that is often found in regions of active normal faulting. Normal-fault footwalls formed in resistant rock are often rimmed with prominent bedrock fault scarps that range in

[1]Cooperative Institute for Research in Environmental Sciences and Department of Geological Sciences, University of Colorado, Boulder, Colorado, USA.
[2]Department of Earth Science and Engineering, Royal School of Mines, Imperial College, London, UK.
[3]Department of Earth and Planetary Sciences, Birkbeck College, London, UK.
[4]Department of Geosciences and Institute for Water and Watersheds, Oregon State University, Corvallis, Oregon, USA.
[5]School of Earth and Environment, University of Leeds, Leeds, UK.

0148-0227/11/2010JF001861

height from meters to a few tens of meters. Bedrock scarps have been recognized, for example, along normal faults in central Italy [e.g., *Giraudi*, 1995], Greece [*Armijo et al.*, 1992], the western United States (e.g., Teton, Watach, and Great Basin faults) [*Smith et al.*, 1993; *Byrd et al.*, 1994; *DePolo and Anderson*, 2000; *Smith and Siegel*, 2000; *Machette et al.*, 2001], and southern Tibet [*Armijo et al.*, 1986]. In the case of the Mediterranean and western U.S. regions, bedrock footwall scarps have been interpreted to represent accumulated offset following the last glacial maximum [*Dufaure*, 1977; *Armijo et al.*, 1992; *Pierce and Good*, 1992; *Byrd et al.*, 1994; *Piccardi et al.*, 1999; *Morewood and Roberts*, 2000; *Machette et al.*, 2001; *Roberts and Michetti*, 2004]. Exposure-age dating of carbonate fault scarps in southern Greece [*Benedetti et al.*, 2002] and central Italy [*Palumbo et al.*, 2004; *Schlagenhauf*, 2009; *Schlagenhauf et al.*, 2010] confirms this view. The selective preservation of bedrock fault scarps is widely believed to reflect a dramatic reduction in hillslope erosion rates under the warmer postglacial climate [e.g., *Armijo et al.*, 1992; *Piccardi et al.*, 1999; *Morewood and Roberts*, 2000].

[4] The apparently rapid breakdown of newly formed scarps under glacial climate conditions, and their widespread preservation under interglacial climate, presents an opportunity to quantify the degree of climatic control on bedrock weathering across a glacial-interglacial cycle. Here we use a combination of morphological analysis, weathering-pit measurements, and mathematical modeling to document glacial-interglacial variations in hillslope erosion rate on a normal-fault footwall in the Central Apennines of Italy. In order to estimate the long-term average hillslope erosion rate, we derive a simple geometric model of weathering and erosion on the steep flank of a normal-fault footwall and apply this model to the well-constrained Magnola fault. The geometric model implies that the hillslope angle is set by the fault dip and by the ratio of slip rate to slope-normal erosion rate, and it can in principle be applied to any active normal faults with planar, bedrock-dominated hillslope facets. To explore the consequences of varying erosion rates through time, we develop a numerical implementation of the footwall-erosion model and compute the topography that would be expected if the late Pleistocene and Holocene erosion rate tracked the global oxygen isotope curve. Finally, to constrain Holocene erosion rates, we report measurements of weathering pits on a carbonate fault scarp whose exposure age is constrained by cosmogenic ^{36}Cl analysis. With this combined analysis we demonstrate a strong climatic control on bedrock weathering and erosion rates.

2. Field Setting and Fault Scarp Observations

2.1. Overview

[5] The Italian Central Apennines (Figure 1a, inset) have been undergoing NE-SW extension since the Pliocene to early Pleistocene, following an earlier period of compression and crustal shortening related to southwestward subduction of the Adria microplate [*Anderson and Jackson*, 1987; *Patacca et al.*, 1990; *Doglioni*, 1993; *Jolivet et al.*, 1998; *Cavinato and Celles*, 1999]. Active extension has been accompanied by broad-wavelength uplift across the peninsula [*D'Agostino et al.*, 2001], with the result that many of the hanging wall basins now lie several hundred meters above mean sea level.

[6] The mean monthly temperature in central Abruzzo ranges between 1.7° and 18.7°C (based on gridded data by *New et al.* [2002] at grid point 42°5′N, 13°25′E), while the mean annual temperature is 9.6°C. The mean monthly precipitation ranges from 56 to 106 mm with an autumn maximum. Mean annual precipitation is 906 mm.

[7] We focus here on the region northeast of Rome (Figure 1a, inset). Lithology in the region consists predominantly of Mesozoic and Cenozoic carbonates in the footwalls, and a combination of carbonates, fine-grained clastic rocks, and Neogene alluvial and lacustrine facies in the hanging wall basins. Bedrock fault scarps, ranging in height from meters to a few tens of meters, commonly rim the footwalls of active normal faults (Figures 1b, 2, and 3b). The scarps are decorated by fault striations, indicating that they represent exhumed sections of the fault planes. Because these scarps are considered to be postglacial features, their height has been used to estimate the postglacial slip rate on faults throughout the region [*Piccardi et al.*, 1999; *Galadini and Galli*, 2000; *Morewood and Roberts*, 2000; *Roberts et al.*, 2002; *Roberts and Michetti*, 2004; *Papanikolaou et al.*, 2005]. Several lines of evidence demonstrate that these bedrock scarps are postglacial. Similarity in height between bedrock scarps and scarps formed on nearby last-glacial moraines and fluvio-glacial fans support the inference that the bedrock scarps represent postglacial offset [*Morewood and Roberts*, 2000]. In addition, where Holocene throw rates have been estimated from paleoseismic trench studies, the rates are consistent with those derived from bedrock scarp height [*Pantosti et al.*, 1996; *Morewood and Roberts*, 2000]. Finally, exposure-age dating of fault scarps using cosmogenic ^{36}Cl yields postglacial ages [*Palumbo et al.*, 2004; *Schlagenhauf*, 2009; *Schlagenhauf et al.*, 2010].

2.2. Magnola Fault: Geomorphic Setting

[8] We focus on the well-studied Magnola fault, an approximately 12 km long, ESE striking active normal fault that marks the southern edge of the carbonate Magnola Mountains (Figure 1). The Magnola fault's footwall, together with that of the adjacent Velino fault, supports some of the highest topography in the region. Monte Velino, at 2487 m ASL, forms the highest peak in the range. Both footwalls show well-developed triangular facets (Figure 1).

[9] *Palumbo et al.* [2004] used cosmogenic ^{36}Cl to reconstruct the detailed exposure history of a portion of the scarp along the Magnola fault, near the village of Forme (referred to hereafter as the Forme site; Figure 2). These data were extended and reanalyzed by *Schlagenhauf et al.* [2010], who accounted for several additional influences on the ^{36}Cl production rate. The results of their study imply that samples near the top of the ~7 m high (~10 m along plane) smooth and well-preserved portion of the basal scarp (as opposed to the degraded upper portions [*Faure Walker et al.*, 2009]) have been exposed for about 7.2 ka, supporting the widely held view that these scarps are postglacial features. They also concluded that the well-preserved portion of the scarp reflects a minimum of five earthquakes. However, a related study by the same authors [*Schlagenhauf*, 2009] suggested that the top of the smooth portion of

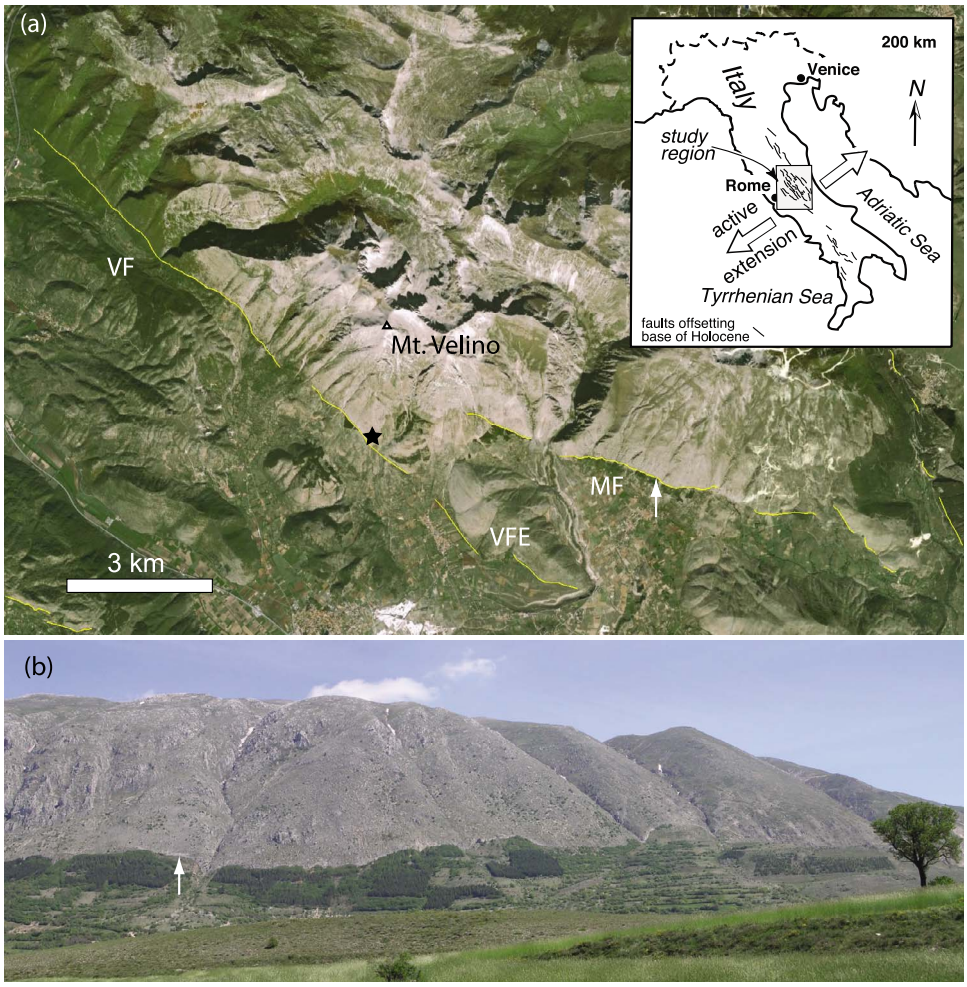

Figure 1. (a) Satellite image of the Velino-Magnola massif, showing surface trace of Magnola (MF) and Velino (VF and VFE) faults (light-colored lines along mountain base). Google Earth imagery ©Google Inc. Used with permission. (b) Photograph of the Magnola mountain front (courtesy P. Cowie). White arrows in Figures 1a and 1b indicate Forme sampling site (approximately 42.1195°N, 13.4485°E).

the scarp at Forme might be as young as 4.8 ka, based on the assumption that the slip history at Forme must match the inferred slip history at four other sites along the Velino and Magnola faults. Together the two approaches imply a scarp-top exposure age at Forme between 4.4 and 8.0 ka, with the range reflecting the mean age for the two different models plus 1σ analytic uncertainties. The corresponding average

Figure 2. The Magnola scarp at the Forme site, looking to the northeast. The sampling site of *Palumbo et al.* [2004] is visible as a white, 20 cm wide band on the scarp at center left. The relatively smooth scarp face in the center and left is typical of scarps in the region (photo by S. McCoy).

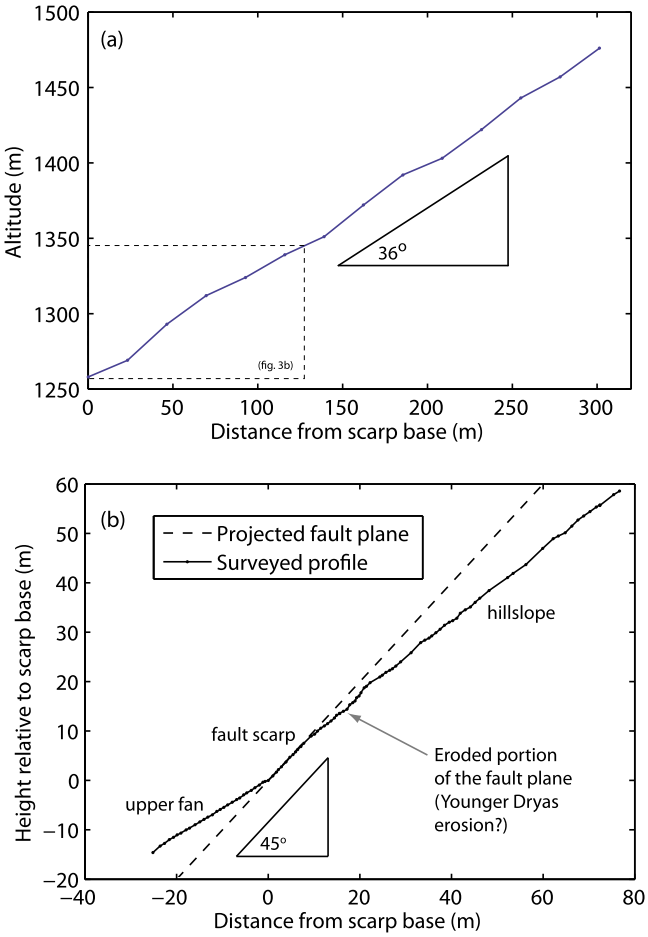

Figure 3. (a) Topographic profile of planar hillslope above the fault at Forme, derived from 20 m digital elevation model. (b) Projected fault plane and topographic profile of upper fan, fault scarp, and lower hillslope at the Forme site, obtained with laser survey instrument.

throw rate since the mid-Holocene to late Holocene falls in the range of 1.0 to 1.8 mm/yr.

[10] *Piccardi et al.* [1999] reported that the facets immediately above the bedrock scarp along the Magnola fault range in slope from 28° to 35°, while average fault dip is approximately 55°. At the sampling site studied by *Palumbo et al.* [2004] and *Schlagenhauf et al.* [2010], the fault dip is 45° ± 2° and the mountain front facet slope is 36° (Figure 3). The difference between the fault dip and the mountain-front (facet) slope angle implies that the slopes have undergone considerable erosion since being generated by progressive fault slip. Estimates of erosion depth as a function of height above the fault are presented below.

2.3. Regolith Production and Transport

[11] The thickness and spatial distribution of soil cover can provide information on the nature of hillslope erosion and sediment transport. Hillslopes that are mantled with a continuous soil cover are commonly assumed to be transport limited, whereas those with extensive areas of bare bedrock are considered to be weathering limited [*Carson and Kirkby*, 1972]. Carbonate facet slopes in the Central Apennines tend to have quite thin soils, on the order a few decimeters or less, with a large fraction of exposed bedrock (Figures 1b and 2). Above the Magnola fault in particular, the facet hillslopes consist of a mosaic of exposed bedrock patches separated by shallow pockets of soil and rock debris. To quantify soil thickness, we excavated soil pits at 10 m intervals along a transect above the Forme site, parallel to the fall line. In order to describe the short-wavelength variability, at each site along the transect we measured the maximum soil thickness and estimated the percentage of exposed bedrock within a 1 m radius circle. The average slope-normal thickness (weighted by the percentage soil cover within 1 m) ranges from 0 to 15 cm (Figure 4). Bare rock was always exposed within 1 m of each sample location. The data show no systematic trend in thickness with distance along slope.

[12] The thin and patchy soil cover on these facet slopes suggests that using standard diffusion-based models to describe footwall evolution [e.g., *Petit et al.*, 2009a] would be inappropriate for this setting because such models assume an essentially unlimited supply of mobile sediment. Furthermore, the hillslopes above the Velino and Magnola faults also show no evidence of bedrock landsliding, which has also been proposed as a key process in other normal-fault-bounded ranges [*Densmore et al.*, 1998]. Instead, the mountain-front slopes are generally planar and smooth (on a length scale greater than a few meters), and exhibit no landslide headscarps, runout debris, or failure planes. Similar steep, thinly mantled slopes formed on carbonate footwalls occur throughout the Central Apennines [e.g., *Roberts and Michetti*, 2004] as well as the Peloponnese in southern Greece [e.g., *Armijo et al.*, 1992].

[13] Dry ravel [e.g., *Gabet*, 2003] appears to be an important sediment-transport process on footwall hillslopes in the Central Apennines, based on the abundance of loose rock debris and sheets and shallow cones of scree, and the observation that the angle of the rocky footwall slopes is often equal to or greater than the apparent angle of repose

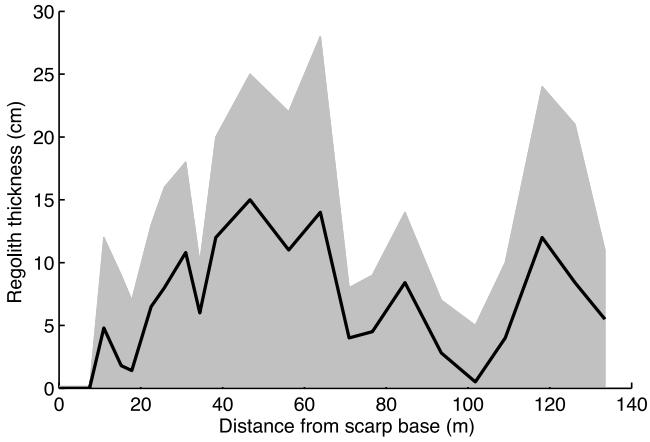

Figure 4. Slope-normal regolith thickness measured in soil pits excavated every 10 m above the scarp base near the Forme sample site. Grey shading encompasses the range of regolith thickness at each site. The thick black line is the weighted mean, which was calculated by multiplying the regolith thickness measurements by the visually estimated percentage of regolith-covered ground area within 1 m of the sample site.

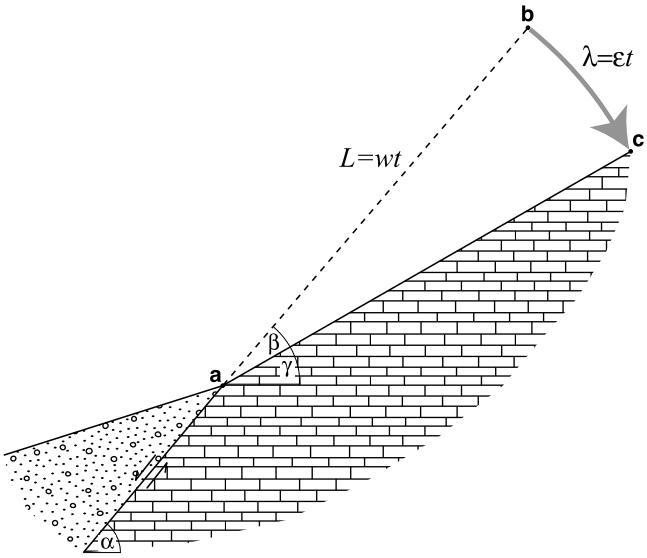

Figure 5. Schematic illustration of the geometry of a planar normal-fault facet or mountain-front slope; α is the fault dip, γ is the hillslope angle, and β is the difference between them. L represents the accumulated fault displacement between points a and b, over a time period t; λ represents the cumulative slope-normal erosion depth at point c over the same time period; w is the fault slip rate; and ϵ is the average slope-normal erosion rate.

for loose scree. Dislodgment by moving animals may also contribute to downslope sediment transport. The high fracture density of the carbonate bedrock seems to preclude significant overland-flow erosion under the present-day climate. However, frozen ground during glacial periods may have allowed for enhanced runoff and overland-flow erosion, as hypothesized, for example, for northern Europe [*Bogaart et al.*, 2003]. Evidence for periglacial conditions in the Central Apennines during the last glaciation is discussed, for example, by *Giraudi and Frezzotti* [1997].

3. Methods

3.1. Geometric Model for Mountain Front Erosion and Facet Slope Angle

[14] The difference in angle between the fault plane and the facet slopes can be used to estimate the thickness of rock that has been eroded at any point on the facet. Consider a point on the fault plane rupture surface that daylights during an earthquake (Figure 5, point a). If there were no erosion, then after a time period t the point would be translated a total distance $L = wt$, where w is the fault slip rate (Figure 5, point b). With erosion, however, the corresponding point on the facet surface will undergo a total depth of erosion λ during the same time interval, in the direction perpendicular to the slope (Figure 5, point c). The slope-normal erosion depth λ at any point on the mountain front hillslope equals the arc of a circle of radius L that subtends an angle β, equal to the difference between the fault plane angle, α, and the hillslope angle, γ. Expressing angles in radians,

$$\lambda = (\alpha - \gamma)L. \tag{1}$$

The average erosion rate ϵ during time interval t is simply

$$\epsilon = \lambda/t. \tag{2}$$

Therefore, if the fault slip rate $w = L/t$ is known, the erosion rate can be derived from (1) as

$$\epsilon = (\alpha - \gamma)w. \tag{3}$$

The equation above indicates that the slope-normal erosion rate is simply equal to the fault slip rate times the difference in angle between the fault plane and the hillslope. Note that w and ϵ are average rates, and short-term variability over time in both will tend to introduce corresponding variability in slope morphology. Assuming for the sake of argument that slip and erosion rates have a stationary, long-term average (that is, for example, that the slip rate has a constant average value at timescales longer than the earthquake recurrence interval), then any short-term variations would become increasingly averaged out over time, with higher parts of the facet slopes representing a longer averaging period.

[15] Note also that if the erosion rate were independently known, the fault slip rate could also be obtained from $w = \epsilon/(\alpha - \gamma)$. We will revisit this point in section 5.5.

3.2. Numerical Model of Facet Slope Evolution

[16] A simple numerical model allows us to explore hillslope evolution on the steep mountain-front slope above an active normal fault, and in particular to examine cases in which erosion rate varies over time. The model captures what we consider to be two essential elements of bedrock facet slope evolution: (1) each earthquake both raises and lengthens the mountain front, creating a fault scarp at the slope base that then begins to erode, and (2) erosion takes place in the direction perpendicular to the slope. The surface-normal erosion rate ϵ is initially assumed to be independent of slope angle. Such an assumption might seem surprising, given that sediment flux on soil-mantled slopes is known to depend strongly on slope angle [e.g., *Roering et al.*, 2001; *Roering*, 2008]. However, in this case the assumption is justified by the thin, patchy regolith cover on facet slopes in the Central Apennines and Greece (Figures 1, 2, and 4). The patchy regolith cover on the mountain-front slopes suggests that erosion is effectively limited by the rate of regolith production from bedrock, rather than by the capacity to transport regolith downslope. We assume therefore that the mountain-front slopes are weathering limited in the sense defined by *Carson and Kirkby* [1972], with regolith being shed essentially as fast as it is produced.

[17] The hillslope is represented mathematically as a two-dimensional parametric curve with horizontal coordinate $x(s)$ and vertical coordinate $z(s)$, where s represents distance along the curve. Use of a parametric curve, rather than a single value of height for each distance increment, allows points to undergo fault offset and erosion in both the vertical and horizontal directions. The local slope angle at point s is $\gamma(s)$. Erosion rate is expressed by its vertical and horizontal components. The vertical component of erosion at a point s is equal to the slope-normal component ϵ times the cosine of the local slope angle,

$$-\frac{\partial z(s)}{\partial t} = \epsilon \cos\gamma(s). \tag{4}$$

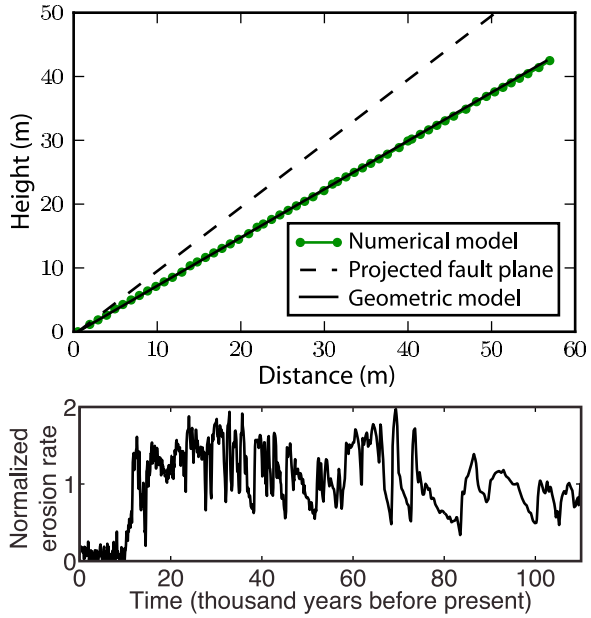

Figure 6. (top) Mountain front facet computed by numerical model for 50,000 years of fault slip and erosion, compared with projected fault plane and hillslope angle and length predicted by geometry. Parameters are $w \sin \alpha$ = 1 mm/yr; ϵ = 0.2 mm/yr; T_e = 1000 yr; δ = 2 m; Δt = 10 years; and α = 45°. (bottom) Erosion rate curve, based on a linear transform of the GISP2 oxygen-isotope curve, used in model calculations with time varying erosion. Vertical axis shows erosion rate normalized by its mean.

Similarly, the horizontal component of erosion depends on the sine of slope angle,

$$\frac{\partial x(s)}{\partial t} = \epsilon \sin \gamma(s). \tag{5}$$

[18] In the numerical model, the hillslope is divided into a set of points. The height z and horizontal position x of each point will move over time in response to (1) offset during earthquakes (each of which is represented as an instantaneous shift up and to the right for points at or below the projected fault plane) and (2) erosion (which is represented as a gradual shift down and to the right for each point). The points initially form a horizontal surface with a point spacing of δ meters. Time is discretized into a sequence of time steps of duration Δt years. During each time step, erosion is calculated by shifting points vertically and laterally using the forward difference approximations:

$$z_i^{t+1} = z_i^t - \epsilon \cos \gamma_i^t \Delta t \tag{6}$$

$$x_i^{t+1} = x_i^t + \epsilon \sin \gamma_i^t \Delta t, \tag{7}$$

where, for example, z_i^t is the elevation at point i at time t. The local slope angle γ is calculated using a weighted average of the four neighboring points. (Note that points with a slope angle less than a threshold of 10° are considered too gentle to erode; this simply has the effect of preventing initially horizontal points from eroding below the fault trace.)

[19] Fault motion is treated as a discrete, episodic process. Earthquakes occur with a recurrence interval T_e and produce vertical and lateral offsets at all points below the projected fault plane of $\Delta z = wT_e \sin \alpha$ and $\Delta x = \Delta z/\tan \alpha$, respectively. When the gap between any pair of points grows larger than twice the nominal spacing δ, a new point is added between the two points. Similarly, when two points come within half the nominal spacing of one another, they are replaced by a single point at their midpoint.

[20] When the erosion rate is constant in time and space, the model produces a planar mountain front with a length $L = wt$ and a slope angle $\gamma = \alpha - (\epsilon/w)$ (Figure 6, top), as predicted by the geometric model illustrated in Figure 5. The numerical model also allows us to explore morphologic consequences of a time varying erosion rate. In particular, we wish to know whether this model, when driven with a reasonable fault slip rate and a simple proxy for regional glacial-interglacial temperature variations, is sufficient to explain the observed quasi-planar ~36° slopes with well-preserved ~10 m high fault scarps at their bases. To establish a hypothetical relationship between erosion rate and climate, we assume that erosion rate tracks the oxygen isotope record from the GISP2 ice core [*Grootes et al.*, 1993; *Grootes and Stuiver*, 1997]. Late Pleistocene pollen records from Lago Grande di Monticchio in southern Italy [*Allen et al.*, 1999; *Huntley et al.*, 1999; *Allen et al.*, 2000] and Lago dell'Accesa in central Italy [*Drescher-Schneider et al.*, 2007] show a close correspondence with the GISP2 oxygen isotope curve. In particular, environmental reconstruction based on pollen from the Monticchio cores indicates a rapid change in environment near the beginning of the Holocene, with the mean temperature of the coldest month warming from −5 to +3°C in as little as a few hundred years [*Allen et al.*, 2000], consistent with the GISP2 record.

[21] To transform the ~110,000 year oxygen isotope curve into an erosion rate, we use

$$\epsilon(t) = (\bar{\epsilon} - \epsilon_{\min}) \frac{\max(D) - D(t)}{\langle \max(D) - D(t) \rangle} + \epsilon_{\min}, \tag{8}$$

where $D(t)$ is the oxygen isotopic value at a particular time t, $\bar{\epsilon}$ is the average erosion rate, $\epsilon_{\min}$ is the minimum erosion rate, and the angle brackets denote the mean. The erosion-rate function is shown in Figure 6 (bottom).

[22] Our use of a temperature-dependent proxy is based on the presumption that the processes most likely to drive regolith generation in this setting are temperature sensitive. Frost shattering in particular is known to be highly temperature-dependent [*Walder and Hallet*, 1985; *Anderson*, 1998], and as discussed further in section 5, it is likely to be the most important rock-weathering process in this setting.

3.3. Measurement of Holocene Erosion on the Magnola Fault Scarp

[23] Weathering and erosion on the Magnola fault scarp involve chemical alteration of the scarp surface [*Carcaillet et al.*, 2008] as well as disintegration through the formation of pits and fractures. Based on the scarp morphology and climate-vegetation environment, it is likely that rock breakdown involves a combination of calcite dissolution, root growth, and seasonal frost wedging. To quantify the

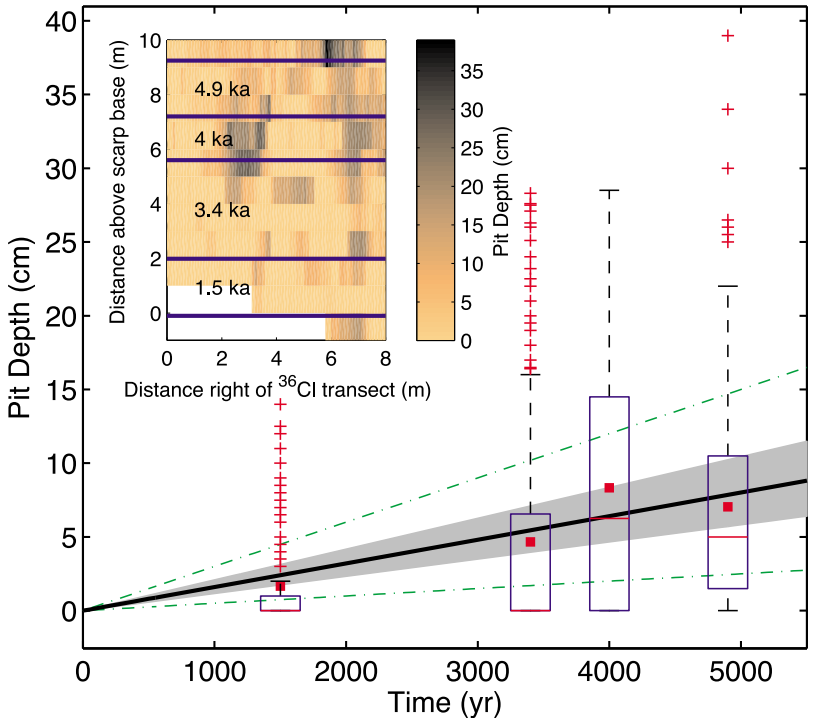

Figure 7. Box-whisker plot of average pit depth within each age band on Magnola scarp near Forme. Areas without pits are recorded as having zero depth, so that the depth plotted represents an average over the entire scarp face. Top and bottom of each box show 25th and 75th percentiles, respectively. Red center lines in boxes are medians (note the younger age band distributions are heavily skewed toward 0 cm pit depth, so the medians plot on the bottom of the box). Squares show means. Whiskers extend up to 1.5 times the interquartile range. Points beyond whiskers are plotted individually as crosses. Thick black line shows zero-intercept linear regression fit to means of each age band (slope is 0.016 mm/yr; $r^2 = 0.79$). Grey shading encompasses the sum of errors due to pit-depth measurement and scarp-age uncertainty ±0.005 mm/yr. Slopes of green dash-dotted lines encompass the range of modern limestone weathering rates from around Italy (0.005 to 0.03 mm/yr) [*Furlani et al.*, 2009; *Stephenson and Finlayson*, 2009]. Inset shows digital relief model of scarp derived from pit measurements, with darker colors showing deeper pitting. Areas of no data (white) were covered with colluvium. Ages and locations of age bands are from *Schlagenhauf* [2009].

rate of mass removal by weathering and erosion during the Holocene we used the detailed scarp exposure history determined by *Palumbo et al.* [2004], *Schlagenhauf* [2009], and *Schlagenhauf et al.* [2010] to partition the fault scarp into sections of the same age. We then used a tape measure and calipers to measure the distribution of pit depths within each age class (Figure 7, inset).

[24] To measure the distribution of pit depths, the scarp was divided into a grid with 1.0 m spacing up the fault plane and 0.1 m spacing along the strike of the scarp. The origin of the grid was at the intersection of the vertical ^{36}Cl sampling transect of *Palumbo et al.* [2004] and the contact between the alluvial fan and fault scarp. A measuring tape was stretched 8.0 m perpendicular to the ^{36}Cl sampling transect and anchored tightly. Where the scarp surface was smooth, the tape rested against the scarp; where the scarp was pitted due to weathering and erosion the tape was elevated above the scarp surface. Pit depths below the tape datum were then measured with calipers every 10 cm horizontally along the tape. When one horizontal transect was complete the tape was moved 1 m up the scarp, up to a maximum along-scarp height of 9.0 m. A conservative estimate of the accuracy of the pit depth measurements was ±1 cm. A digital terrain model of the scarp surface was then made (Figure 7, inset).

[25] The preferred exhumation history of *Schlagenhauf et al.* [2010] consists of five rapid exhumation events, with offset in each event ranging from 1.6 m to 3.6 m. These events are assumed to record either individual large earthquakes or closely spaced (in time) clusters of smaller events. The oldest event exhumed the portion of the scarp above 9.25 ± 0.3 m, which is above our highest horizontal transect at 9.0 m. Hence, the ages of events that exhumed the portion of the scarp we measured are 1.5, 3.4, 4.0, and 4.9 ka, each with an average uncertainty of ~±0.5 ka. Other model interpretations fall within these error bands for these four events [*Schlagenhauf*, 2009]. These age bands are plotted in Figure 7 (inset).

[26] To determine a minimum erosion rate averaged over the last ~5 ka of the Holocene, the slope of a linear regression through the mean pit depth of each age band was calculated. These rates are minimum estimates because we assume that the smooth unpitted portion of the scarp (the zero pit depth datum) is not eroding, or is eroding extremely slowly. This is a reasonable assumption given preserved

slickensides on various smooth portions of the scarp. The gray shading around the regression line (Figure 7) encompasses the sum of errors due the uncertainty in measured pit depth (±1 cm) and the uncertainty in the age of each band of the scarp (±0.5 ka). Note that older ages [e.g., *Faure Walker et al.*, 2009] would reduce both the Holocene scarp erosion rate and the inferred longer-term erosion rate, and therefore would not change the relative difference between them.

4. Results

4.1. Holocene Erosion Rate on the Magnola Scarp

[27] Despite the evident variability in pitting depth and frequency along the scarp face, the data show a clear trend in mean depth with increasing scarp-face age (Figure 7). Linear regression through the weathering-pit data implies an average scarp erosion rate of 0.016 ± 0.005 mm/yr. This estimate falls within the range of erosion rates measured over much shorter timescales (~20 years) on limestones in northeastern Italy and Slovenia (0.005–0.03 mm/yr) [*Furlani et al.*, 2009; *Stephenson and Finlayson*, 2009].

[28] The measurable uncertainty in the erosion rate is almost equally divided between uncertainty in the pit depth measurement and uncertainty in the age of the scarp. The uncertainty due to our assumption that the smooth parts of the scarps are not eroding is more difficult to quantify. The preservation of slickensides on the scarp suggests that the erosion rate of the smooth part of the scarp is less than the typical relief of a slickenside (several millimeters) divided by the age of the scarp; this suggests a maximum erosion rate on the order of 0.001 mm/yr. A worst case could arguably be that the smooth parts of the scarp are also eroding uniformly at a rate near the maximum modern rate of 0.03 mm/yr. This would imply a maximum possible Holocene erosion rate of 0.051 mm/yr, but even this low rate is likely to be an overestimate.

4.2. Long-Term Erosion Rate Above the Magnola Scarp

[29] The long-term average erosion rate of the hillslope at Forme can be estimated using equation (3), given the fault dip, hillslope angle, and fault throw rate. Measurement of the scarp and lower hillslope profile using a laser survey instrument (Figure 3b) indicates that the fault scarp dips at ~45° while the slope angle immediately above the scarp is 36.5°. A 300 m long hillslope profile extracted from a 20 m resolution DEM at the same location reveals a slope angle of 35.8° (Figure 3a). A cosmogenic exposure age of 7.2 ka (+0.8/−1.0) ka at the Forme site was obtained at a distance of 9.25 m updip of the scarp base [*Schlagenhauf et al.*, 2010], which corresponds to a height of 6.5 m vertically above the scarp base. *Schlagenhauf et al.* [2010] interpreted this date as representing the base of a ~1.9 m long (1.3 m high) slip surface. Using the top of this surface (at 6.5 + 1.3 = 7.8 m vertically above the fault) to represent the total accumulated offset, and applying as bounding values the 1σ error estimates, the corresponding average fault throw rate (equal to slip rate multiplied by the sine of fault dip angle) ranges from 1.0 to 1.3 mm/yr. With these throw rates and assuming a hillslope angle of $\gamma = 36°$, equation (3) implies a long-term hillslope erosion rate between 0.22 and 0.28 mm/yr.

[30] Interpreting seismic history and exposure ages from ^{36}Cl measurements necessarily involves some ambiguity. In this case, a study by *Schlagenhauf* [2009, chap. 5] combined data from the Forme site with data from four other sites along the Magnola and Velino faults to derive two alternative seismic histories that honor data at all five of the sample sites. One of the two models reaffirmed an upper scarp age at Forme between 7 and 8 ka. A second model, which requires each site to have the same slip history, suggested a much younger scarp-top exposure age of 4.8 (+0.7/−0.4) ka. The corresponding fault throw rate for the latter model ranges from 1.4 to 1.8 mm/yr. Between the two models, and accounting for 1σ uncertainty bands for each, the throw rate on the Magnola fault at the Forme site may be as little as 1.0 or as high as 1.8 mm/yr. Applying those rates in equation (3) yields an average erosion rate between 0.22 and 0.40 mm/yr. Regardless of which model is closer to the true slip history, these results demonstrate that the late Pleistocene average erosion rate must be at least an order of magnitude higher than both the estimated Holocene rate and the contemporary carbonate weathering rates documented by monitoring studies.

[31] To estimate the amount of time that this average rate represents, we can divide the height of the hillslope profile shown in Figure 3a (about 200 m) by the fault throw rate. For the throw rate derived by *Schlagenhauf et al.* [2010] of 1.0–1.3 mm/yr, rocks that are now at the top of the profile in Figure 3a would have been at the same altitude as the fault trace between 150 and 200 thousand years ago. For the higher throw rate (1.8 mm/yr), the time span would be closer to 110 kyr. Thus, our estimated erosion rate represents an average over approximately one to two glacial cycles.

4.3. Glacial-Interglacial Variations in Hillslope Erosion Rate and Their Morphologic Consequences

[32] The numerical model described in section 3.2 allows us to explore how time variation in the rate of hillslope erosion influences slope morphology. Figure 8 shows a model run using an erosion-rate history based on the GISP2 isotope curve, with a mean erosion rate of 0.24 mm/yr, a post-7.2 ka average rate of 0.022 mm/yr, and a fault slip rate of 1.55 mm/yr. It is important to emphasize that these parameters were derived directly from data rather than being fit to the profile. The fault slip rate comes from the cosmogenic exposure-age data of *Schlagenhauf et al.* [2010], and is derived from the fault plane-parallel distance to the top of the 7.2 ka slip surface (11.15 m) divided by its age. The mean erosion rate comes from using this fault slip rate in equation (3) with a fault-dip angle of 45° and a hillslope angle of 36°. The Holocene erosion rate is chosen to fall within the range suggested by the Forme weathering pit data and by the results of limestone dissolution-rate studies discussed above; it falls on the high end of the range simply because a smaller value would have caused the Holocene portion of our linear erosion-rate curve (Figure 6, bottom) to dip below zero too frequently (even with the higher rate, there are a few oscillations that dip below zero; we handle this by simply setting any negative values to zero).

[33] The modeled profile resembles the field-surveyed hillslope profile at Forme (Figure 8). As expected, the model hillslope shows a prominent convexity near the base of the slope. This convexity, which represents the preserved fault

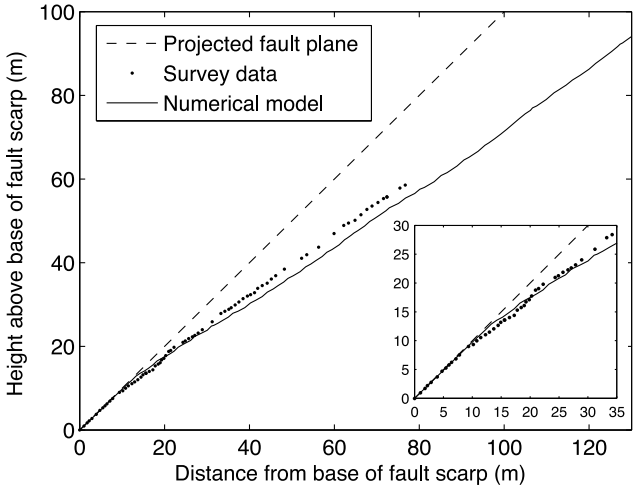

Figure 8. Numerical simulation of hillslope evolution using erosion rate driven by GISP2 oxygen isotope curve, compared with surveyed hillslope profile. Inset shows close-up view of basal scarp. Parameters are: throw rate is $w \sin \alpha = 1.095$ mm/yr; $\alpha = 45°$; $\bar{\epsilon} = 0.243$ mm/yr; average erosion rate over the past 7.2 ky is 0.022 mm/yr; $\delta = 1$ m; $\Delta t = 1$ year; and $T_e = 1000$ years.

scarp, records the Holocene reduction in erosion rate. Both the modeled and observed upper hillslopes are about 9° gentler than the fault plane. Variations in erosion rate over time produce subtle undulations in the modeled hillslope profile, with steeper segments corresponding to periods of reduced erosional intensity. The measured hillslope profile shows an abrupt slope break at approximately 18 m above the base of the scarp. The equivalent slope break in the modeled profile is somewhat lower, between about 13 and 16 m above the scarp base. Such a discrepancy is not surprising given the observed meter-scale variation in scarp height (Figure 2) and the simplifying assumptions used in the model (uniform lithology, constant earthquake interval, and linear erosion-temperature relation). For our purposes, the important finding is that the model predicts a quasi-planar hillslope that has a lower slope angle than the fault plane and a preserved 10–20 m high fault scarp at its base.

[34] Using different combinations of erosion rate and fault slip rate (such as $\epsilon = 0.04$ mm/yr and $w = 2.5$ mm/yr) has little effect on the solution as long as the predicted average hillslope angle (from equation (3)) remains the same. Likewise, changing the earthquake interval has little effect apart from altering the smoothness of the profile (which tends to be slightly smoother when earthquakes are smaller and more frequent, as one would expect). The run shown in Figure 8 is representative of a family of solutions with $\gamma_{\text{average}} = 36°$.

5. Discussion

[35] The estimated rates of weathering and erosion at the Magnola mountain front suggest a strong sensitivity to climate, with rates varying by more than an order of magnitude between glacial and interglacial periods. When these rates are used to drive a simple model of erosion and episodic slip on a normal-fault footwall, the model predicts a hillslope morphology consisting of a quasi-planar slope that has at its base a much steeper scarp whose height represents accumulated postglacial slip. Together, these two findings support the hypothesis that scarp preservation on normal-fault footwalls in the Central Apennines reflects a roughly order-of-magnitude decrease in hillslope weathering and erosion rates since the last glacial maximum.

[36] This interpretation raises the question of what mechanisms for weathering and erosion of fault scarps and mountain-front hillslopes in the carbonate ranges of the Central Apennines are likely to have been most important during the last few hundred thousand years. A related issue is the question of whether there are plausible alternatives to a climatic interpretation. These issues are considered in sections 5.1 and 5.2.

5.1. Weathering Processes

[37] Of the various possible rock-weathering mechanisms on the steep, semiarid carbonate hillslopes in the Apennines, the most obvious candidates are (1) carbonate dissolution, (2) stresses created by plant root growth and dislodgment ("tree throw"), and (3) frost wedging. Dissolution is certain to play some role in weakening the footwall rocks. Many of the carbonate outcrops in the region show features characteristic of dissolution, such as pits and shallow furrows. In addition, many of the Pleistocene gravel-rich fans and fluvial deposits in the Central Apennines show strong cementation, implying elevated calcite concentration in groundwater. However, the popular karst denudation model of *White* [1984], analyzed by *Ford and Williams* [2007], implies that solutional denudation of limestone is only weakly sensitive to temperature, while empirical data suggest that solutional dissolution rates are typically lower under colder climates [*Ford and Williams*, 2007, Figure 4.3]. The model also implies that solution rate is sensitive to soil pCO_2, which tends to be higher where vegetation is more dense because of the increased flux from roots and microbes [e.g., *Schaetzl and Anderson*, 2005]. Vegetation reconstructions based on the Monticchio pollen record in southern Italy [*Allen et al.*, 2000] and from Lake Accesa in Tuscany [*Magny et al.*, 2006] imply reduced, not increased, vegetation density during late Pleistocene cold intervals. Thus, it is highly unlikely that dissolution alone could have produced a major increase in rock breakdown rate during cold periods. A further piece of evidence against dissolution as the leading process is the abundance of angular limestone fragments on hillslopes and fans in the region, which suggests a substantial component of physical weathering.

[38] Plant-driven rock breakdown is also inconsistent with reduced weathering during interstadial periods. The Monticchio and Accesa pollen records show dramatic changes in the relative proportions of woody and herbaceous species, with grasses and other herbaceous species predominant during cold periods [*Allen et al.*, 2000; *Drescher-Schneider et al.*, 2007]. Rock disruption by tree throw and woody root growth ought therefore to be most active during warm periods, which again is inconsistent with the apparent acceleration in rock disintegration rates during cold, steppe-dominated periods.

[39] When the ground temperature falls below freezing, growth of ice lenses can exert considerable stresses within rock. Under the right temperature and moisture conditions,

these stresses are strong enough to drive fracturing. This frost cracking process reflects not simply the ~9% expansion of water upon freezing, but rather the sustained growth of ice lenses as liquid groundwater migrates toward them [*Walder and Hallet*, 1985]. Frost cracking is most effective when ground temperature lies between −3° and about −8°C, given sufficient moisture supply [*Anderson*, 1998; *Walder and Hallet*, 1985].

[40] Were the central Apennines cold and wet enough to drive frost wedging during glacial periods? *Allen et al.* [2000] used the Monticchio pollen record to reconstruct the mean temperature of the coldest month (MTCO) and the ratio of actual to potential evapotranspiration (AET/PET) over the past 110 thousand years for southern Italy. Their reconstruction shows MTCO hovering within the −5° to −10°C range for the majority of oxygen isotope stages 2–4 (~74–13 ka), though with occasional peaks below and (more rarely) above that range [*Allen et al.*, 1999]. Near the start of the Holocene the record shows an abrupt rise to +3°C. For the mid-Holocene and late Holocene, MTCO at Monticchio ranges between +5° and +9°C. Today, the mean January temperature near the Magnola fault, approximately 130 km north of and 600 m higher than Monticchio, is +1.7°C [*New et al.*, 2002]. It appears therefore that near-surface soil temperatures spent considerably more time within the "frost cracking window" during glacial periods than they do today, and thus had the potential for rapid rock disintegration by ice wedge growth.

[41] Frost cracking also requires a moisture supply within the bedrock. Although the Monticchio record suggests generally drier conditions during last glacial period, there are two reasons to suspect that sufficient moisture would have been available to drive frost wedging. First, a reconstruction of the lake-level history at Lago Fucino (a large, now-drained lake basin about 15 km south-southeast of the Magnola fault) shows that the highest lake levels coincided with cold stages [*Giraudi*, 1989], which presumably reflects decreased evapotranspiration. This suggests that soil moisture may have remained relatively high under cold conditions despite reduced precipitation. Second, seasonally or perennially frozen ground may have trapped moisture in the shallow subsurface (the active layer), making it available to migrate to a freezing front. In summary, given the temperature regimes and moisture availability, frost wedging could have played a dominant role in breaking up carbonate bedrock during glacial periods.

5.2. Possible Alternatives to Climate Forcing

[42] One potential challenge to our interpretation is the possibility that there is a strong contrast in weathering rate between a fresh scarp and a substantially degraded one, such that the weathering rate would tend to accelerate as the scarp degrades. Such autogenic acceleration could potentially produce scarps along the base of footwall slopes even without any climatic variation. Here, we use field data to assess whether this alternative hypothesis is viable.

[43] Three considerations suggest that weathering rates could increase as a scarp degrades. First, a degraded scarp will trap water more efficiently, due to a combination of lower slope, rougher texture, and more regolith. Second, the eroded hillslopes above scarps tend to host more vegetation than the scarps themselves (Figures 1b and 2). Finally, the outer portions of carbonate fault surfaces in the Apennines are often armored by a hard, cemented outer layer of fault gouge several centimeters to decimeters thick [*Agosta and Aydin*, 2006]. For example, *Carcaillet et al.* [2008] documented a 1–15 cm thick hardened outer layer at the Forme site, and showed that weathering during subaerial exposure leads to further calcite recrystallization on the exposed scarp face. All of these factors suggest the possibility of a "humped weathering curve," in which bedrock breakdown rate is relatively slow on a fresh fault scarp, and faster when the rock surface lies beneath a shallow cover of regolith [e.g., *Anderson*, 2002]. At issue is whether such a contrast could, by itself, explain the preservation of Holocene fault scarps and the relatively abrupt break in slope and apparent erosion rate between scarps and the hillslopes above them.

[44] A strong contrast in weathering rate between bare rock and shallowly buried rock ought to leave a clear morphologic signature: bedrock fault planes just beneath the soil surface on a fault that has not ruptured for hundreds of years should show significant signs of weathering. At the Forme site, the analysis of *Schlagenhauf* [2009] points toward the last major (>1 m) rupture event as having occurred at least a millennium ago. If, for example, the weathering rate were maximized at 0.25 m depth at a rate of 0.3 mm/yr, one should see a 30 cm thick zone of weathering, at that depth. Instead, excavation of a 4 m long trench by *Schlagenhauf et al.* [2010] revealed a smooth and essentially intact fault surface. Likewise, our own excavations of fault planes at four other sites in Abruzzo show similarly smooth, unweathered fault surfaces at depth. Furthermore, geochemical analysis by *Carcaillet et al.* [2008] suggested that weathering in the shallow subsurface (~20–50 cm) during the lifetime of the Forme fault scarp has been largely limited to reprecipitation of translocated dissolution products at the fault plane surface. These observations imply that the modern rate of rock breakdown beneath the soil that covers the fault plane must be much lower than our derived late Pleistocene average rate of 0.2–0.4 mm/yr. While this inference does not necessarily invalidate the possibility of a positive feedback between regolith cover and rock breakdown rate at our field site, it does imply that the rates associated with such a feedback in the modern weathering environment are far too low to account for the ~9° difference in angle between the hillslope and the fault plane.

[45] A second alternative explanation derives from the observation that rocks within a few tens of centimeters of a carbonate fault plane are often more indurated than the surrounding rocks [*Agosta and Aydin*, 2006]. A substantial acceleration in weathering rate over time, as deeper and possibly softer rocks are progressively exhumed, could potentially produce a convex scarp-to-hillslope profile similar to those observed. However, monitoring data on limestone weathering in the Mediterranean militate against such an interpretation. *Furlani et al.* [2009] presented data from inland and coastal monitoring sites in the northeastern Adriatic region. Data from their 48 inland sites yielded an average limestone lowering rate of 0.018 ± 0.0065 mm/yr over time periods ranging from two to 26 years. Other limestone weathering data from the Mediterranean region, reviewed by *Stephenson and Finlayson* [2009], include measurements from the former Yugoslavia (0.026–0.102 mm/yr over 4 years [*Kunaver*, 1979]), Friuli and

Venezia Giulia, Italy (0.01–0.19 mm/yr over 5 years [*Forti*, 1984] and 0.01–0.04 mm/yr over 15 years [*Cucchi et al.*, 1994]), and Trieste, Italy (also 0.01–0.04 mm/yr over 15 years [*Cucchi et al.*, 1996]). These rates are generally comparable to our estimated Holocene weathering rate for the Forme scarp (Figure 7), and substantially lower than our estimated long-term average rate of 0.2 to 0.4 mm/yr. Thus, we can rule out the hypothesis that scarp preservation arises simply from a rock hardness contrast.

[46] A final and related possibility is that the rock weathering rate increases dramatically over time as a fracture network develops on the scarp face, allowing greater water penetration and increasing the number of ice-lens growth sites. Laboratory experiments on rock fracture by ice segregation by *Murton et al.* [2006] showed an abrupt acceleration in the rate of bedrock dislocation associated with the transition from microcracking to macrocracking. However, the time required to reach this threshold was on the order of hundreds of days (corresponding to tens of temperature cycles), and there is no reason to believe that the timescale in a natural setting would be four orders of magnitude slower than that of the laboratory.

[47] In sum, then, our consideration of possible autocyclic mechanisms leads us to conclude that none of these can account for the observed geometry and age of the fault scarps and hillslopes above them. Instead, climatically controlled variation in the rate of rock breakdown by frost cracking appears to provide the best explanation for our observations.

5.3. Effects of Time-Varying Erosion Rate

[48] When computing erosion rate based on the GISP2 oxygen isotope curve, the numerical model produces a hillslope morphology that resembles the Magnola hillslopes, with a steep scarp at the base of a relatively straight ~36° slope, on which are superimposed gentle undulations (Figure 8). However, the model scarp differs in detail from the real one, notably in lacking an upper, partially degraded portion. Several factors could account for the discrepancy. First, the model uses a fixed earthquake recurrence interval with a constant slip per event, which obviously differs in detail from the actual sequence inferred from ^{36}Cl and geochemical analysis of the scarp face [*Palumbo et al.*, 2004; *Carcaillet et al.*, 2008; *Schlagenhauf*, 2009; *Schlagenhauf et al.*, 2010]. Second, our use of a linear transformation between the GISP2 curve and the hillslope erosion rate (equation (8)) is a significant simplification. For example, if frost wedging is the dominant process, one might expect a strong response as mean winter temperatures dip into the −3° to −10°C frost cracking window, but little additional increase (and possibly a decrease) when mean January temperature drops below −10°C (as the Monticchio record implies that they did periodically). In that light, the dip in temperature recorded at ~8.2 ka (the "8.2 ka event") is interesting. This event correlates with a lake-level highstand at Lake Accesa in Tuscany, suggesting a period of wetter conditions [*Magny et al.*, 2006]. It is conceivable that increased moisture availability around 8.2 ka drove enhanced winter frost wedging responsible for degradation of those parts of the fault scarp that were exposed at the time (i.e., those older than 8200 years). Such an interpretation is consistent with the first of two age models considered by *Schlagenhauf* [2009], in which three of four sites along the Magnola fault have preferred scarp-top ages between 7 and 8 ka.

[49] A third potential explanation for the discrepancy between the observed and modeled scarp height lies in small-scale spatial variability in rock susceptibility to weathering. Indeed, some spatial variability in scarp weathering is implied by the older ^{36}Cl ages obtained at one of the four Magnola sites (11.4 and 13.7 ka for models "opt" and "max," respectively) [*Schlagenhauf*, 2009]. A final possibility is that we have underestimated the interseismic interval. If, for example, one or more closely spaced earthquakes had occurred between the last glacial maximum and the Younger Dryas, and if the fault had then remained stable for several thousand years, the scarp could have experienced significant degradation. Such a scenario could also account for the upper, degraded portion of the scarp observed at Forme (Figures 3 and 8).

5.4. Implications for Climatic Control on Erosion

[50] Using a linear transformation between the GISP2 isotope record ("climate") and erosion rate implies that the maximum erosion rate over the past 100–200 ka was about thirty times higher than the modern rate of scarp weathering. Such a dramatic rate contrast provides some support for the hypothesis that global climate cooling led to a widespread increase in mountain erosion rates [*Molnar and England*, 1990]. It suggests in particular that high-relief regions that were drawn into the "frost cracking window" during the late Cenozoic could have experienced order-of-magnitude increases in rates of rock weathering, at least under conditions similar to those of the Central Apennines: steep slopes, shallow regolith, sufficient near-surface ground moisture, and hard rocks. This suggestion is also consistent with evidence from the New Zealand Southern Alps that rates of scree production reach a maximum at altitudes within the optimum temperature range for frost wedging [*Hales and Roering*, 2005].

5.5. Applying the Footwall Erosion Model to Other Faults

[51] The criteria for using the geometric model to estimate erosion rate at other sites include: planar mountain-front hillslopes (facets) with little or no regolith cover and absence of bedrock landsliding, a known fault plane dip, and a known fault slip rate. The first set of conditions (morphology) seems to apply to many normal-fault-bounded mountain fronts, such as those in the Peloponnesian region [*Dufaure*, 1977; *Armijo et al.*, 1992], southern Tibet [*Armijo et al.*, 1986], the Baikal Rift [*Petit et al.*, 2009b], and much of the North American extensional province. The biggest limitation lies in constraining fault slip rates.

[52] Conversely, in regions where rates of rock weathering and erosion can be independently derived, the method can in principle be used to derive long-term average fault slip rates from facet slope angle. The most straightforward application would be to a single fault system on homogeneous rock, such that spatial variation in rock disintegration rate would be minimized. For example, if a single fault in homogeneous rock had a fixed length over a given period of time (i.e., its tips were temporarily pinned), both the slip rate and cumulative slip during that time period would be

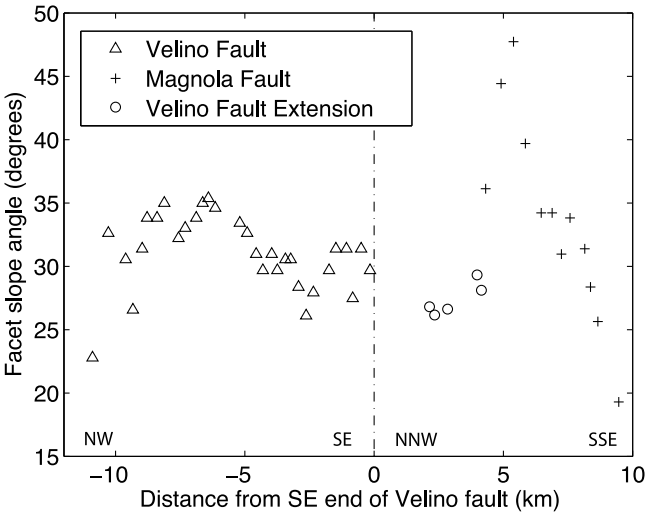

Figure 9. Facet slope angles along the Velino and Magnola faults. Slope angles were measured from 20 m digital elevation model, using ~300 m long transects starting at the approximate position of the fault and following the steepest straight line upward. Horizontal axis represents euclidean distance from the position where the Velino and Magnola mountain fronts join (black star in Figure 1a; UTM E365,750, N4,665,270, datum EUR1950, zone 33). Circles show the southeastward extension of the Velino fault (VFE in Figure 1a).

expected to tend to zero at the fault tips. The theory illustrated in Figure 5 predicts that, all else being equal, the slip-rate profile in such a case should be reflected in the facet slope angles. A preliminary test of this prediction is shown in Figure 9, which plots facet slope angle as a function of position along the Velino and Magnola faults. The facet slope angle tends to decrease toward the northwestern tip of the Velino fault as well as toward the eastern tip of the Magnola fault, consistent with a decline in slip rate toward the fault tips. The three unusually steep points toward the western end of the Magnola fault lie near the flanks of the glacial Majelama valley, and are likely to be influenced by rapid base level lowering due to valley incision. The peak in slope angle toward the center of the Velino fault suggests that the fault's slip rate is maximized at that location, which is what would be expected if it were not linked with the Magnola fault. On the other hand, the decline in facet slope angle along the Velino fault is less pronounced toward the southeast end than toward the northwest end. This could reflect either partial linkage with the Magnola fault, or the likelihood that the Velino fault overlaps the Magnola along the line of hills to the south ("VFE" in Figure 1a).

[53] Although the data in Figure 9 are not conclusive, the pattern suggests that the facet slope angles may indeed broadly reflect the fault slip rates integrated over a timescale of order 10^5 years. A stronger test will require a fault with an unusually well-characterized late Quaternary slip-rate profile, combined with high-resolution topographic data. One important caveat is that the hillslope angle is not set by the slip rate directly, but rather by the rate of exhumation of the fault plane, which can be influenced by net erosion or deposition in the hanging wall [*Whittaker et al.*, 2007] as well as by the dip and strike of the fault plane [*Faure Walker et al.*, 2009]. For that reason it is important to identify locations where the footwall has been relatively stable over the time period of interest, and to document carefully the local fault plane geometry.

6. Conclusions

[54] The existence of well-preserved Holocene bedrock fault scarps along active normal faults in the Mediterranean region and elsewhere suggests a strong reduction in rates of rock weathering and erosion that correlates with the transition from glacial to interglacial climate. Alternative hypotheses for scarp preservation, including accelerated weathering under a thin soil mantle and tectonic hardening of rocks lining the fault plane, are considered unlikely; the first implies rapid fault plane weathering in the shallow subsurface, which is not observed, while the second is inconsistent with regional data on rates of limestone weathering. Thus, scarp preservation is interpreted to reflect late Quaternary climate change.

[55] A simple geometric analysis of normal-fault slip and erosion implies that the slope angle of normal-fault facets is set by the slip rate, fault dip angle, and average rate of erosion during the period of subaerial exposure. Therefore, if the slip rate and fault dip are known, the average erosion rate can be estimated. Similarly, if the erosion rate is known, the slip rate can be estimated. Application of the method to the Magnola fault suggests an average erosion rate on the order of a few tenths of a millimeter per year over the past one to two glacial cycles. The range reflects uncertainties in the fault slip rate as deduced from cosmogenic ^{36}Cl exposure dating.

[56] Analysis of the scarp and facet morphology allows us to quantify the contrast in weathering and erosion rates between glacial and interglacial periods. Measurement of weathering features on the Magnola bedrock fault scarp, where previous ^{36}Cl exposure dating provides age control, yields an estimated weathering rate on the order of hundredths of a millimeter per year. This rate is consistent with inland limestone weathering rates measured in the northern Adriatic region, and it is an order of magnitude slower than the estimated long-term rate.

[57] The large difference between Holocene and late Pleistocene rates of rock breakdown implies a strong climatic control on hillslope weathering and erosion rates. This interpretation is supported by calculations with a numerical model of fault motion and erosion, in which erosion rate is hypothesized to mirror the GISP2 oxygen-isotope curve. The model generates hillslope morphology consistent with that of the Magnola mountain front.

[58] We hypothesize that frost cracking acts as the dominant mechanism for rock breakdown. Previous work has shown the process to be most effective when the ground temperature lies between −3° and −10°C. Sustained temperatures this low are uncommon in the region today even during winter, but a climate reconstruction based on a long pollen record from southern Italy suggests that mean January temperatures at the Magnola Mountains fell within or below this range during the last glacial period. The suggestion that frost cracking acts as an important geomorphic

agent in the Apennines is interesting in light of the recognition of the role of frost cracking in other rocky environments [*Hales and Roering*, 2005, 2007, 2009; *Delunel et al.*, 2010].

[59] If our interpretation is correct, it suggests an important connection between erosion rates and climate. Specifically, regions that experience a climatic cooling sufficient to bring the ground temperatures into the "frost cracking window" could potentially see a substantial increase in rates of hillslope erosion and sediment production. In that sense, our data are consistent with the hypothesis that global climate cooling drove widespread increases in mountain erosion rates during the late Cenozoic [*Molnar and England*, 1990]. The mechanism applies specifically to rocky landscapes thinly mantled with soil (so that the rock-regolith interface is not insulated against seasonal temperature swings) and with steep slopes (so that regolith generated by frost cracking is efficiently eroded).

[60] The prediction that facet slope reflects a combination of erosion rate and fault slip rate implies that if one knew the erosion rate independently, one could estimate the fault slip rate. An interesting implication is that a normal fault whose tips are pinned should, all else being equal, show a systematic decline in facet angle toward the fault tips. A preliminary test using the Velino and Magnola faults is broadly consistent with this prediction.

[61] **Acknowledgments.** This research was supported by grants from the U.S. National Science Foundation (EAR-0643240 to Tucker and EAR-0643353 to Lancaster) and NERC (GR9/02995, NE/B504165/1, NE/E01545X/1, and NE/H003266/1). G.E.T. is also grateful to the Centre National de la Recherche Scientifique for support during a sabbatical visit to the Université Joseph Fourier in Grenoble, France. GISP2 oxygen isotope data were provided by the National Snow and Ice Data Center, University of Colorado at Boulder, and the WDC-A for Paleoclimatology, National Geophysical Data Center, Boulder, Colorado. We thank Nate Bradley for help in collecting survey data at the Magnola scarp and Mikael Attal for kindly reviewing an early draft. Alex Densmore, Manny Gabet, George Hilley, and an anonymous reviewer provided very helpful review comments. Last but not least, is a pleasure to acknowledge ongoing collaboration and discussions with Patience Cowie.

References

Agosta, F., and A. Aydin (2006), Architecture and deformation mechanism of a basin-bounding normal fault in Mesozoic platform carbonates, central Italy, *J. Struct. Geol.*, *28*(8), 1445–1467.

Allen, J., et al. (1999), Rapid environmental changes in southern Europe during the last glacial period, *Nature*, *400*(6746), 740–743.

Allen, J., W. Watts, and B. Huntley (2000), Weichselian palynostratigraphy, palaeovegetation and palaeoenvironment; The record from Lago Grande di Monticchio, southern Italy, *Quaternary Int.*, *73–74*, 91–110.

Anderson, H., and J. Jackson (1987), Active tectonics of the Adriatic region, *Geophys. J. R. Astron. Soc.*, *91*(3), 937–983.

Anderson, R. (1998), Near-surface thermal profiles in alpine bedrock: Implications for the frost weathering of rock, *Arct. Alp. Res.*, *30*(4), 362–372.

Anderson, R. (2002), Modeling the tor-dotted crests, bedrock edges, and parabolic profiles of high alpine surfaces of the Wind River Range, Wyoming, *Geomorphology*, *46*(1–2), 35–58.

Armijo, R., P. Tapponnier, J. Mercier, and T. Han (1986), Quaternary extension in southern Tibet: Field observations and tectonic implications, *J. Geophys. Res.*, *91*(B14), 13,803–13,872.

Armijo, R., H. Lyon-Caen, and D. Papanastassiou (1992), East-west extension and Holocene normal-fault scarps in the Hellenic arc, *Geology*, *20*(6), 491–494.

Benedetti, L., R. Finkel, D. Papanastassiou, G. King, R. Armijo, F. Ryerson, D. Farber, and F. Flerit (2002), Post-glacial slip history of the Sparta fault (Greece) determined by ^{36}Cl cosmogenic dating: Evidence for non-periodic earthquakes, *Geophys. Res. Lett.*, *29*(8), 1246, doi:10.1029/2001GL014510.

Bogaart, P., G. Tucker, and J. De Vries (2003), Channel network morphology and sediment dynamics under alternating periglacial and temperate regimes: A numerical simulation study, *Geomorphology*, *54*(3–4), 257–277.

Bull, W. B. (2001), *Geomorphic Responses to Climatic Change*, Blackburn Press, Caldwell, N. J.

Byrd, J., R. Smith, and J. Geissman (1994), The Teton fault, Wyoming: Topographic signature, neotectonics, and mechanisms of deformation, *J. Geophys. Res.*, *99*(B10), 20,095–20,122.

Carcaillet, J., I. Manighetti, C. Chauvel, A. Schlagenhauf, and J. Nicole (2008), Identifying past earthquakes on an active normal fault (Magnola, Italy) from the chemical analysis of its exhumed carbonate fault plane, *Earth Planet. Sci. Lett.*, *271*(1–4), 145–158.

Carson, M. A., and M. J. Kirkby (1972), *Hillslope Form and Processes*, Cambridge Univ. Press, Cambridge, U. K.

Cavinato, G., and P. Celles (1999), Extensional basins in the tectonically bimodal central Apennines fold-thrust belt, Italy: Response to corner flow above a subducting slab in retrograde motion, *Geology*, *27*(10), 955–95.

Coulthard, T. J., and M. J. Kirkby (2002), Simulating upland river catchment and alluvial fan evolution, *Earth Surf. Processes Landforms*, *27*, 269–288.

Cucchi, F., F. Fabio, and F. Ulcigrai (1994), Degradation by dissolution of carbonate rocks, *Acta Carsol.*, *23*, 55–62.

Cucchi, F., F. Fabio, and E. Marinett (1996), Surface degradation of carbonate rocks in the karst of Trieste (Classical Karst, Italy), in *Karren Landforms*, edited by J.-J. Fornós and À. Ginés, pp. 41–51, Univ. Illes Balears, Palma, Spain.

D'Agostino, N., J. Jackson, F. Dramis, and R. Funiciello (2001), Interactions between mantle upwelling, drainage evolution and active normal faulting: An example from the central Apennines (Italy), *Geophys. J. Int.*, *147*(2), 475–497.

Delunel, R., P. van der Beek, J. Carcaillet, D. Bourles, and P. Valla (2010), Frost-cracking control on catchment denudation rates: Insights from *in situ* produced ^{10}Be concentrations in stream sediments (Ecrins-Pelvoux massif, French Western Alps), *Earth Planet. Sci. Lett.*, *293*(1–2), 72–83.

Densmore, A. L., M. A. Ellis, and R. S. Anderson (1998), Landsliding and the evolution of normal-fault-bounded mountains, *J. Geophys. Res.*, *103*, 15,203–15,219.

DePolo, C., and J. Anderson (2000), Estimating the slip rates of normal faults in the Great Basin, USA, *Basin Res.*, *12*(3–4), 227–240.

Doglioni, C. (1993), Some remarks on the origin of foredeeps, *Tectonophysics*, *228*(1–2), 1–20.

Drescher-Schneider, R., J. de Beaulieu, M. Magny, A. Walter-Simonnet, G. Bossuet, L. Millet, E. Brugiapaglia, and A. Drescher (2007), Vegetation history, climate and human impact over the last 15,000 years at Lago dell'Accesa (Tuscany, Central Italy), *Veg. Hist. Archaeobot.*, *16*(4), 279–299.

Dufaure, J. (1977), Neotectonique et morphogenese dans une peninsule mediterraneenne, Le Peloponnese, *Rev. Geogr. Phys. Geol. Dyn.*, *19*(1), 27–58.

Faure Walker, J., G. Roberts, P. Cowie, I. Papanikolaou, P. Sammonds, A. Michetti, and R. Phillips (2009), Horizontal strain-rates and throw-rates across breached relay zones, central Italy: Implications for the preservation of throw deficits at points of normal fault linkage, *J. Struct. Geol.*, *31*(10), 1145–1160.

Ford, D., and P. Williams (2007), *Karst Hydrogeology and Geomorphology*, John Wiley, Chichester, U. K.

Forti, F. (1984), Messungen des karsrabtrages in der region friul-julische-venetien (Italian), *Die Hohle*, *35*, 125–139.

Furlani, S., F. Cucchi, F. Forti, and A. Rossi (2009), Comparison between coastal and inland Karst limestone lowering rates in the northeastern Adriatic region (Italy and Croatia), *Geomorphology*, *104*(1–2), 73–81.

Gabet, E. (2003), Sediment transport by dry ravel, *J. Geophys. Res.*, *108*(B1), 2049, doi:10.1029/2001JB001686.

Galadini, F., and P. Galli (2000), Active tectonics in the Central Apennines (Italy)–Input data for seismic hazard assessment, *Nat. Hazards*, *22*(3), 225–268.

Giraudi, C. (1989), Lake levels and climate for the last 30,000 years in the fucino area (Abruzzo-Central Italy)—A review, *Palaeogeogr. Palaeoclimatol. Palaeoecol.*, *70*(1–3), 249–260.

Giraudi, C. (1995), Considerations on the significance of some post-glacial fault scarps in the Abruzzo Apennines (Central Italy), *Quat. Int.*, *25*, 33–45.

Giraudi, C., and M. Frezzotti (1997), Late Pleistocene glacial events in the Central Apennines, Italy, *Quat. Res.*, *48*(3), 280–290.

Grootes, P., and M. Stuiver (1997), Oxygen 18/16 variability in Greenland snow and ice with 10^{-3}- to 10^{5}-year time resolution, *J. Geophys. Res.*, *102*(C12), 26,455–26,470.

Grootes, P., M. Stuiver, J. White, S. Johnsen, and J. Jouzel (1993), Comparison of oxygen isotope records from the GISP2 and GRIP Greenland ice cores, *Nature*, *366*(6455), 552–554.

Hales, T., and J. J. Roering (2005), Climate-controlled variations in scree production, Southern Alps, New Zealand, *Geology*, *33*(9), 701–704.

Hales, T., and J. J. Roering, (2007), Climatic controls on frost cracking and implications for the evolution of bedrock landscapes, *J. Geophys. Res.*, *112*, F02033, doi:10.1029/2006JF000616.

Hales, T., and J. J. Roering, (2009), A frost "buzzsaw" mechanism for erosion of the eastern Southern Alps, New Zealand, *Geomorphology*, *107*(3–4), 241–253.

Hancock, G. S., and R. S. Anderson (2002), Numerical modeling of fluvial strath-terrace formation in response to oscillating climate, *Geol. Soc. Am. Bull.*, *114*, 1131–1142.

Hovius, N. (1998), Controls on sediment supply by large rivers, *Spec. Publ. SEPM Soc. Sediment. Geol.*, *59*, 3–16.

Huntley, B., W. Watts, J. Allen, and B. Zolitschka (1999), Palaeoclimate, chronology and vegetation history of the Weichselian Lateglacial: comparative analysis of data from three cores at Lago Grande di Monticchio, southern Italy, *Quat. Sci. Rev.*, *18*, 945–960.

Jolivet, L., et al. (1998), Midcrustal shear zones in postorogenic extension: Example from the northern Tyrrhenian Sea, *J. Geophys. Res.*, *103*(B6), 12,123–12,160.

Kirkby, M. J., and N. Cox (1995), A climatic index for soil erosion potential, *Catena*, *25*, 333–352.

Kunaver, J. (1979), Some experiences in measuring the surface karst denudation in a high alpine environment, in *Actes du Symposium International sur l'erosion karstique: Aix-en-Provence-Marseille-Nîmes, 10–14 Septembre 1979*, pp. 75–85, Assoc. Fr. de Karstol., Mus. Hist. Nat., Paris.

Leeder, M. R., T. Harris, and M. J. Kirkby (1998), Sediment supply and climate change: Implications for basin stratigraphy, *Basin Res.*, *10*, 7–18.

Machette, M., K. Pierce, J. McCalpin, K. Haller, and R. Dart (2001), Map and data for Quaternary faults and folds in Wyoming, *U.S. Geol. Surv. Open File Rep., 01-461*, 158 pp.

Magny, M., J. de Beaulieu, R. Drescher-Schneider, B. Vanniere, A. Walter-Simonnet, L. Millet, G. Bossuet, and O. Peyron (2006), Climatic oscillations in central Italy during the Last Glacial-Holocene transition: the record from Lake Accesa, *J. Quaternary Sci.*, *21*(4), 311–320.

Milliman, J. D., and P. M. Syvitski (1992), Geomorphic/tectonic control of sediment transport to the ocean: The importance of small mountainous rivers, *J. Geol.*, *100*, 525–544.

Molnar, P. (2004), Late cenozoic increase in accumulation rates of terrestrial sediment: How might climate change have affected erosion rates?, *Annu. Rev. Earth Planet. Sci.*, *32*, 67–89.

Molnar, P., and P. England (1990), Late Cenozoic uplift of mountain ranges and global climate change—Chicken or egg?, *Nature*, *346*(6279), 29–34.

Morewood, N., and G. Roberts (2000), The geometry, kinematics and rates of deformation within an en echelon normal fault segment boundary, central Italy, *J. Struct. Geol.*, *22*(8), 1027–1047.

Murton, J., R. Peterson, and J. Ozouf (2006), Bedrock fracture by ice segregation in cold regions, *Science*, *314*(5802), 1127.

New, M., D. Lister, M. Hulme, and I. Makin (2002), A high-resolution data set of surface climate over global land areas, *Clim. Res.*, *21*(1), 1–25.

Palumbo, L., L. Benedetti, D. Bourles, A. Cinque, and R. Finkel (2004), Slip history of the Magnola Fault (Apennines, Central Italy) from ^{36}Cl surface exposure dating: Evidence for strong earthquake over the Holocene, *Earth Planet. Sci. Lett.*, *225*, 163–176.

Pantosti, D., G. D'Addezio, and F. Cinti (1996), Paleoseismicity of the Ovindoli-Pezza fault, central Apennines, Italy: A history including a large, previously unrecorded earthquake in the Middle Ages (860–1300 AD), *J. Geophys. Res.*, *101*(B3), 5937–5959.

Papanikolaou, I., G. Roberts, and A. Michetti (2005), Fault scarps and deformation rates in Lazio-Abruzzo, Central Italy: Comparison between geological fault slip-rate and GPS data, *Tectonophysics*, *408*(1–4), 147–176.

Patacca, E., R. Sartori, and P. Scandone (1990), Tyrrhenian basin and Apenninic arcs: Kinematic relations since late Tortonian times, *Mem. Soc. Geol. Ital.*, *45*(1), 425–451.

Petit, C., Y. Gunnell, N. Gonga-Saholiariliva, B. Meyer, and J. Séguinot (2009a), Faceted spurs at normal fault scarps: Insights from numerical modeling, *J. Geophys. Res.*, *114*, B05403, doi:10.1029/2008JB005955.

Petit, C., B. Meyer, Y. Gunnell, M. Jolivet, V. San'kov, V. Strak, and N. Gonga-Saholiariliva (2009b), Height of faceted spurs, a proxy for determining long-term throw rates on normal faults: Evidence from the North Baikal Rift System, Siberia, *Tectonics*, *28*, TC6010, doi:10.1029/2009TC002555.

Piccardi, L., Y. Gaudemer, P. Tapponnier, and M. Boccaletti (1999), Active oblique extension in the central Apennines (Italy): Evidence from the Fucino region, *Geophys. J. Int.*, *139*(2), 499–530.

Pierce, K., and J. Good (1992), Field guide to the Quaternary geology of Jackson Hole, Wyoming, *U.S. Geol. Surv. Open File Rep.*, *92*(504), 49.

Riebe, C., J. Kirchner, D. Granger, and R. Finkel (2001), Strong tectonic and weak climatic control of long-term chemical weathering rates, *Geology*, *29*(6), 511–514.

Roberts, G., and A. Michetti (2004), Spatial and temporal variations in growth rates along active normal fault systems: An example from the Lazio-Abruzzo Apennines, central Italy, *J. Struct. Geol.*, *26*(2), 339–376.

Roberts, G., A. Michetti, P. Cowie, N. Morewood, and I. Papanikolaou (2002), Fault slip-rate variations during crustal-scale strain localisation, central Italy, *Geophys. Res. Lett.*, *29*(8), 1168, doi:10.1029/2001GL013529.

Roering, J. J. (2008), How well can hillslope evolution models "explain" topography? Simulating soil transport and production with high-resolution topographic data, *Geol. Soc. Am. Bull.*, *120*(9–10), 1248–1262.

Roering, J. J., J. Kirchner, L. Sklar, and W. Dietrich (2001), Hillslope evolution by nonlinear creep and landsliding: An experimental study, *Geology*, *29*(2), 143–146.

Schaetzl, R., and S. Anderson (2005), *Soils: Genesis and Geomorphology*, Cambridge Univ. Press, Cambridge, U. K.

Schlagenhauf, A. (2009), Identification des forts seismes passes sur les failles normales actives de la region Lazio–Abruzzo (Italie Centrale) par "datations cosmogéniques" (36Cl) de leurs escarpements, Ph.D. thesis, Univ. Joseph Fourier, Grenoble, France.

Schlagenhauf, A., Y. Gaudemer, L. Benedetti, I. Manighetti, L. Palumbo, I. Schimmelpfennig, R. Finkel, and K. Pou (2010), Using *in-situ* chlorine-36 cosmonuclide to recover past earthquake histories on limestone normal fault scarps: a reappraisal of methodology and interpretations, *Geophys. J. Int.*, *182*(1), 36–72.

Smith, R., and L. Siegel (2000), *Windows into the Earth: The Geologic Story of Yellowstone and Grand Teton National Parks*, Oxford Univ. Press, Oxford, U. K.

Smith, R., J. Byrd, and D. Susong (1993), The Teton fault, Wyoming: Seismotectonics, Quaternary history, and earthquake hazards, in *Geology of Wyoming*, *Geol. Surv. Wyo. Mem.*, vol. 5, edited by A. W. Snoke, J. R. Steidtmann, and S. M. Roberts, pp. 628–667, Geol. Surv. of Wyo., Laramie.

Stephenson, W., and B. Finlayson (2009), Measuring erosion with the micro-erosion meter—Contributions to understanding landform evolution, *Earth Sci. Rev.*, *95*(1–2), 53–62.

Summerfield, M., and N. Hulton (1994), Natural controls of fluvial denudation rates in major world drainage basins, *J. Geophys. Res.*, *99*(B7), 13,871–13,883.

Tucker, G. E., and R. L. Slingerland (1997), Drainage basin response to climate change, *Water Resour. Res.*, *33*, 2031–2047.

Walder, J., and B. Hallet (1985), A theoretical model of the fracture of rock during freezing, *Geol. Soc. Am. Bull.*, *96*(3), 336–346.

White, W. (1984), Rate processes: Chemical kinetics and karst landform development, in *Groundwater as a Geomorphic Agent*, edited by R. G. LaFleur, pp. 227–248, Allen and Unwin, Boston, Mass.

Whittaker, A., P. Cowie, M. Attal, G. Tucker, and G. Roberts (2007), Contrasting transient and steady-state rivers crossing active normal faults: New field observations from the Central Apennines, Italy, *Basin Res.*, *19*(4), 529–556.

Zhang, P., P. Molnar, and W. Downs (2001), Increased sedimentation rates and grain sizes 2–4 Myr ago due to the influence of climate change on erosion rates, *Nature*, *410*, 599–604.

S. T. Lancaster, Department of Geosciences, Oregon State University, 104 Wilkinson Hall, Corvallis, OR 97331, USA.

S. W. McCoy and G. E. Tucker, Cooperative Institute for Research in Environmental Sciences and Department of Geological Sciences, University of Colorado, 2200 Colorado Ave., Campus Box 399, Boulder, CO 80305, USA. (gtucker@colorado.edu)

R. Phillips, School of Earth and Environment, University of Leeds, Leeds LS2 9JT, UK.

G. P. Roberts, Department of Earth and Planetary Sciences, Birkbeck College, Gower Street, London WC1E 6BT, UK.

A. C. Whittaker, Department of Earth Science and Engineering, Royal School of Mines, Imperial College, Prince Consort Road, London SW7 2AZ, UK.